

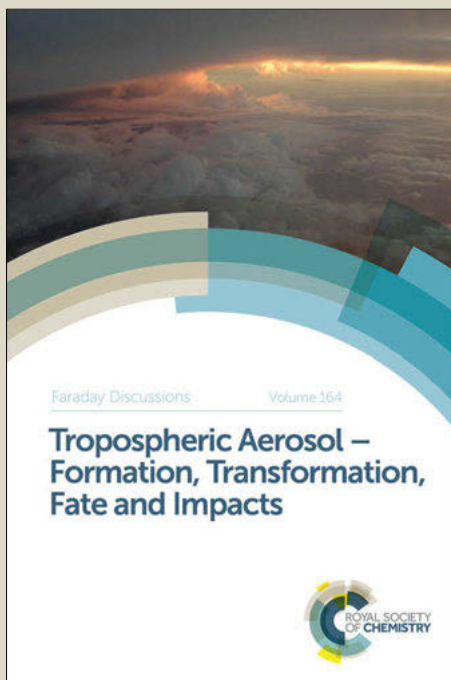
Faraday Discussions

Accepted Manuscript



This manuscript will be presented and discussed at a forthcoming Faraday Discussion meeting. All delegates can contribute to the discussion which will be included in the final volume.

Register now to attend! Full details of all upcoming meetings: <http://rsc.li/fd-upcoming-meetings>



This is an *Accepted Manuscript*, which has been through the Royal Society of Chemistry peer review process and has been accepted for publication.

Accepted Manuscripts are published online shortly after acceptance, before technical editing, formatting and proof reading. Using this free service, authors can make their results available to the community, in citable form, before we publish the edited article. We will replace this *Accepted Manuscript* with the edited and formatted *Advance Article* as soon as it is available.

You can find more information about *Accepted Manuscripts* in the [Information for Authors](#).

Please note that technical editing may introduce minor changes to the text and/or graphics, which may alter content. The journal's standard [Terms & Conditions](#) and the [Ethical guidelines](#) still apply. In no event shall the Royal Society of Chemistry be held responsible for any errors or omissions in this *Accepted Manuscript* or any consequences arising from the use of any information it contains.

SCHOLARONE™
Manuscripts

Capturing interfacial photoelectrochemical dynamics with picosecond time-resolved X-ray photoelectron spectroscopy

Stefan Neppel,^{*a} Andrey Shavorskiy,^a Ioannis Zegkinoglou,^a Matthew
5 Fraund,^a Daniel S. Slaughter,^a Tyler Troy,^a Michael P.
Ziemkiewicz,^a Musahid Ahmed,^a Sheraz Gul,^{bc} Bruce Rude,^a Jin Z.
Zhang,^c Anton S. Tremsin,^d Per-Anders Glans,^b Yi-Sheng Liu,^b
Cheng Hao Wu,^{ef} Jinghua Guo,^b Miquel Salmeron,^c Hendrik
Bluhm,^a and Oliver Gessner^{†a}

10 DOI: 10.1039/b000000x [DO NOT ALTER/DELETE THIS TEXT]

Time-resolved core-level spectroscopy using laser pulses to initiate and short X-ray pulses to trace photoinduced processes has the unique potential to provide electronic state- and atomic site-specific insight into fundamental electron dynamics in complex systems. Time-domain studies
15 using transient X-ray absorption and emission techniques have proven extremely valuable to investigate electronic and structural dynamics in isolated and solvated molecules. Here, we describe the implementation of a picosecond time-resolved X-ray photoelectron spectroscopy (TRXPS) technique at the Advanced Light Source (ALS) and its application to
20 monitor photoinduced electron dynamics at the technologically pertinent interface formed by N3 dye molecules anchored to nanoporous ZnO. Strong indications for a dynamical chemical shift of the Ru3d photoemission line originating from the N3 metal centre are observed ~30 ps after resonant HOMO-LUMO excitation with a visible laser pump pulse. The transient
25 changes in the TRXPS spectra are accompanied by a characteristic surface photovoltage (SPV) response of the ZnO substrate on a pico- to nanosecond time scale. The interplay between the two phenomena is discussed in the context of possible electronic relaxation and recombination pathways that lead to the neutralisation of the transiently oxidised dye after ultrafast
30 electron injection. A detailed account of the experimental technique is given including an analysis of the chemical modification of the nanostructured ZnO substrate during extended periods of solution-based dye sensitisation and its relevance for studies using surface-sensitive spectroscopy techniques.

35 ^a Chemical Sciences Division, Lawrence Berkeley National Laboratory, Berkeley, California, USA

^b Advanced Light Source, Lawrence Berkeley National Laboratory, Berkeley, California, USA

^c Department of Chemistry and Biochemistry, University of California Santa Cruz, Santa Cruz, California, USA

^d Space Sciences Laboratory, University of California Berkeley, Berkeley, California, USA

40 ^e Materials Sciences Division, Lawrence Berkeley National Laboratory, Berkeley, California, USA

^f Department of Chemistry, University of California Berkeley, Berkeley, California, USA

* E-mail : sneppel@lbl.gov

† E-mail : ogessner@lbl.gov

Introduction and motivation

A detailed understanding of charge transfer across molecule-semiconductor junctions is a prerequisite for the successful implementation of many envisioned renewable energy technologies. It is essential for electronic processes underlying novel solar photovoltaics, solar-to-fuel conversions and energy storage technologies. It further plays a central role in the field of molecular electronics. In particular, dye-sensitised solar cells have attracted much attention as a promising low-cost alternative to silicon-based photovoltaic devices.¹ A key process in these photoelectrochemical cells is the optically induced electronic excitation of dye molecules, followed by charge separation through electron injection into a semiconductor. Significant ultrafast spectroscopy efforts have been devoted to gaining a detailed picture of the electron-hole separation and free charge carrier generation dynamics. The vast majority of time-domain studies are based on short optical, infrared, and near-ultraviolet (UV) laser pulses for both triggering and probing the time evolution of the excited electronic states by transient reflectivity, absorption and fluorescence.²⁻⁸ Despite remarkable success in identifying the characteristic time scales that govern the interfacial processes, all-optical methods can only access valence electron orbitals, which are generally distributed over many different atomic centres. This delocalised character of the spectroscopic response often renders a detailed interpretation of pump-probe signals ambiguous, especially in the case of complex composite interfaces.

In principle, a deeper insight may be gained by using probe pulses with photon energies in the X-ray spectral range in order to access element-specific information through the involvement of inner-shell electrons. Extremely short X-ray pulses with durations of <100 attoseconds can nowadays be generated using table-top high-harmonic generation (HHG) in noble gases.⁹ This technique enables time-domain studies with unparalleled temporal resolution and further benefits from the intrinsic synchronisation between the HHG driving laser pulses and the generated X-rays. However, for spectroscopic applications HHG currently provides sufficient photon flux only within a rather limited range of photon energies.^{10, 11}

Free-electron laser (FEL) facilities provide intense sub-100 fs X-ray pulses with tunable photon energies ranging up to 20 keV.¹²⁻¹⁴ Currently operational X-ray FEL facilities, however, typically deliver X-rays with extremely high pulse energies but at comparably low repetition rates (<120 Hz), which can present challenges for photoemission spectroscopy experiments on non-replenishing condensed phase samples.¹⁵

Stationary energy-domain X-ray techniques, such as core-hole clock spectroscopy, have been applied with the goal to probe photoinduced femtosecond electron dynamics in molecule-semiconductor systems from the perspective of individual atomic sites.¹⁶ However, these experiments are not equivalent to time-domain studies involving optical excitations since the charge transfer process is initiated by a resonant core-level to LUMO transition that perturbs the energy-level alignment at the interface more strongly than an optically induced HOMO-to-LUMO transition.¹⁷ In addition, the range of dynamic processes that can be addressed with this technique are dictated by the core-hole lifetime (typically a few femtoseconds) – which limits the general applicability of this approach to monitor interfacial electron

dynamics that proceed on time scales spanning many orders of magnitude.

Many important catalytic and photochemical reactions include steps that proceed on pico-to-nanosecond time scales.^{2, 18-23} The intrinsically pulsed X-ray radiation produced at third-generation synchrotron radiation light sources provides an opportunity for real-time studies of the associated dynamics with pulse repetition rates in the MHz regime. These experiments benefit from very stable synchrotron beam characteristics in combination with a time resolution reaching tens of picoseconds – in principle only limited by the length of the electron bunches in the storage ring.

Over the past decade, picosecond time-resolved X-ray absorption spectroscopy has been implemented at a number of synchrotron radiation facilities.^{21, 22, 24, 25} The technique is now used extensively to uncover dynamics in isolated or solvated molecules, revealing important information about intra-molecular energy-, spin-, and charge-redistribution.²⁴ It has also been successfully employed to monitor laser-induced phase transitions of bulk materials.²⁶ Using electron-beam slicing techniques, the time resolution of these experiments can be further improved to ~150 fs^{27, 28} - albeit at the expense of a significantly reduced X-ray flux.

Compared to these achievements, the application of time-resolved X-ray spectroscopy to surfaces and interfaces is still in a very early stage. Some pioneering studies have employed transient X-ray absorption spectroscopy to monitor photoinduced dynamics at molecule-semiconductor interfaces in colloidal systems.^{25, 29} For applications using extended solid-state surfaces covered by molecular monolayers, time-resolved X-ray photoelectron spectroscopy (TRXPS) is a particularly suitable technique that promises to gain real-time insight into interfacial electron dynamics due to its intrinsically high surface sensitivity. Depth specificity and tunability on the order of single monolayers can be achieved by variation of the photoelectron kinetic energy and the measurement geometry.³⁰ So far, synchrotron- and HHG-based TRXPS has mostly been used to study transient surface photo-voltage (SPV) phenomena at clean or oxidised semiconductor surfaces.³¹⁻³⁶ The group of Kapteyn and Murnane applied TRXPS with photon energies below 50 eV to monitor optically induced changes in the valence electronic structure of oxygen molecules adsorbed on a Pt(111) surface.³⁷ Recently, Heinzmann and co-workers used femtosecond XUV pulses from a HHG source centred near ~95 eV to study light-induced dynamics in an iodo-phenylphenol self-assembled monolayer on Si(100).³⁸ The dynamics probed by inner-shell photoionisation of the iodine tail group are marked by a complex time evolution extending over many picoseconds.

Here we describe the implementation of TRXPS at the Advanced Light Source (ALS) with a time resolution of 70 ps (full-width-at-half-maximum, FWHM) and a usable photon energy range of ~70 eV - 1.5 keV, which grants access to the K-shells of all first row elements and the L and M core levels of many transition metals relevant for photocatalytic applications. The experiment combines the use of a high-repetition rate pump laser with time-stamping electron detection. The potential of the technique to provide atomic-site specific real-time access to complex interfacial electron dynamics is demonstrated using the prototypical molecule-semiconductor system of N3 dye molecules (bis(isothiocyanato)bis(2,2'-bipyridyl-4,4'-dicarboxylato)-ruthenium(II), Fig. 1A) adsorbed on a film of nano-structured ZnO. Photoinduced variations in the Ru3d inner-shell binding energies are presented, which constitute a sensitive probe for the valence electron dynamics in the vicinity of the metal centre of the laser-excited dye molecules. Correlations between the

intramolecular and interfacial electron dynamics and the macroscopic surface photovoltage response of the semiconductor support are discussed. The novel technique provides high quality picosecond TRXPS spectra across pump-probe time delays spanning hundreds of nanoseconds within less than one hour of data acquisition time.

Experimental details

Fig. 1 illustrates the key idea of the TRXPS experiment. A visible laser “pump” pulse promotes electrons from the highest occupied molecular orbital (HOMO) of the N3 chromophore to its lowest unoccupied molecular orbital (LUMO), which is aligned with the conduction band (CB) of the ZnO substrate. The dynamic evolution of the excited-state electronic structure is monitored by recording core-level photoelectron spectra of the N3 molecules as a function of the time delay between the laser excitation and the ionising X-ray “probe” pulse. In the following, we refer to positive (negative) time delays when the optical pump pulse arrives at the sample before (after) the X-ray probe pulse. Since the binding energies of the probed energy levels are sensitive to the local charge densities in the vicinity of the core holes, the local temporal variations of the excited valence charges due to electron injection and recombination processes may be reflected in corresponding transient chemical shifts of the core-level binding energies. The N3/ZnO system constitutes a particularly interesting target for TRXPS, since a comprehensive picture of the competition between different dynamic channels that enhance or limit the interfacial charge injection/recombination has not yet emerged.^{6, 20, 23, 39, 40}

Sample preparation and characterisation

ZnO nanoparticles with an average diameter of 16 nm were synthesised according to a procedure described by Bauer et al. using zinc acetate dihydrate as a precursor.²³ About 0.20 ml of the resulting colloidal nanoparticle-ethanol suspension is spin-coated on a 4 inch p-doped Si(100) wafer. Subsequently, the samples are dried at 60 °C and sintered in air at 380 °C for 30 minutes to generate a nanoporous film. Dye adsorption was performed by immersing the ozone/UV-cleaned ZnO films in a 0.2 mM solution of N3 (Solaronix) in absolute ethanol. Sensitisation times ranging from 2 hours to 6 days have been applied to test their impact on the film composition and the surface-sensitive TRXPS experiments. The resulting dye-sensitised ZnO films were thoroughly rinsed with ethanol to remove excess physisorbed molecules and blown dry in a stream of gaseous nitrogen. Samples were kept in the dark and under nitrogen atmosphere prior to loading them into the vacuum chamber (base pressure $\sim 10^{-5}$ mbar) for characterisation with stationary XPS and the TRXPS measurements. Non-sensitised ZnO films on Si and stainless steel supports have been prepared for reference purposes.

During all XPS and TRXPS experiments, the sample has been scanned with respect to the incident X-ray and laser beam to avoid beam damage of the adsorbed dye molecules. The scan speed was chosen in accordance with X-ray damage tests and optical fluorescence decay measurements.⁴¹

Whereas the interaction of N3 deposited from solution or by electrospray techniques onto single-crystalline and nanostructured TiO₂ has been extensively

characterised with stationary XPS,⁴²⁻⁴⁴ a similar comprehensive understanding of the N3 adsorption on ZnO substrates is still lacking. Compared to optical spectroscopy, sample preparation for TRXPS experiments requires additional considerations. The XPS sampling depth in semiconductors is typically <4 nm for electron kinetic energies <600 eV⁴⁵, which makes TRXPS an intrinsically surface-sensitive technique. However, most N3-sensitisation protocols have been developed and tested using more established all-optical spectroscopies, which mainly sample bulk properties of the dye-sensitised semiconductor electrodes.

Hagfeldt and co-workers reported the formation of dye-Zn²⁺ complexes for ZnO films immersed in solutions of Ru-based chromophores.^{46, 47} Molecules bonded in these aggregates were found to be unable to efficiently inject electrons into the semiconductor conduction band.⁴⁸ The growth of dye-Zn²⁺ complexes involves dissolution of Zn-ions from the ZnO surface, which is driven by the protons in the carboxylic acid ligands.⁴⁷ This mechanism is supported by a recent XAS study, in which an exchange of zinc atoms between ZnO nanoparticles and H₂-protoporphyrins featuring carboxylic acid ligands has been observed, eventually leading to metallisation of the molecules.⁴⁹

Figure 2A shows a stationary XPS spectrum of a nanoporous ZnO electrode that has been exposed to the N3 solution for 2 hours. Only peaks expected from the chemical composition of the N3 molecules and the ZnO substrate are observed. The energy axis was calibrated by setting the binding energy of the Au4f_{7/2} line from a gold sample to 84.0 eV. The C1s region is dominated by a photoemission peak at ~285 eV, which is ascribed to carbon atoms in the pyridine ligands of N3 with much smaller (unresolved) contributions from the carbon atoms in the two thiocyanate (NCS) groups and the 3d_{3/2} component of the Ru3d photoemission doublet.^{43, 50} The C1s emission from the carboxylic acid groups gives rise to an additional peak at ~288.5 eV.

The Ru3d_{5/2} photoelectrons from the N3 metal centre is observed at ~280.6 eV binding energy. The complete Ru3d doublet with a spin-orbit splitting of 4.2 eV⁵¹ is indicated as red shaded area in Fig. 2A. The shape and intensities of all peaks in the C1s region are very similar to spectra reported for N3 deposited *in situ* on TiO₂ using electrospray techniques in an ultra-high vacuum environment.^{42, 50} Furthermore, the N1s emission line has a pronounced tail towards lower binding energies, indicating the presence of nitrogen atoms in at least two different chemical environments – compatible with the molecular structure of N3 (Fig. 1A).^{43, 44, 50}

It is generally accepted that chemisorption of N3 on metal-oxide surfaces involves one or more carboxylic acid groups, while the participation of the thiocyanate ligands in the surface bonding is still a matter of debate and may be influenced by the presence of co-adsorbates.^{52, 53} An involvement of the N3 thiocyanate groups in the N3-TiO₂ binding was proposed based on the observation of two chemically shifted components in the S2p photoemission spectrum.^{44, 50} In contrast, the S2p spectrum shown in Fig. 2A can be satisfactorily fitted by a single sulfur 2p doublet with the well-known spin-orbit-splitting of 1.2 eV⁵¹ (red solid line in Fig. 2A). Moreover, its binding energy is rather close to the S2p line position previously assigned to thiocyanate groups not in contact with the substrate.^{44, 50} This favours a bonding motif for N3/ZnO in which only the carboxylic acid groups exhibit a strong interaction (deprotonation) with the surface, in agreement with a recent DFT study on this system.⁴¹

We find that samples prepared with 2 hours sensitisation time exhibit the highest

homogeneity in surface chemical composition, with <8% variations in the total C1s XPS intensity and less than <5% variations in the relative peak ratios when scanning the X-ray beam across centimetre scale sample areas. These electrodes showed no obvious change in colour compared to the bare ZnO substrate, indicating that dye-adsorption was mainly restricted to the outer surface region of the ZnO. For longer sensitisation times, the increased uptake of N3 into the nanoporous film becomes visible as a characteristic coloration of the electrodes (Fig. 2C). However, as demonstrated in Fig. 2B and D, longer sensitisation times are also accompanied by notable changes in the C1s and Zn2p_{3/2} XPS spectra, respectively: for the 6 day sample, a clear broadening of all peaks in the C1s/Ru3d region in combination with a significantly enhanced emission at ~288.5 eV and a reduction and shift/broadening of the Ru3d_{5/2} emission line is observed. In addition, the Zn2p_{3/2} substrate emission broadens and an additional broad peak appears at ~4 eV higher binding energy compared to the 2 hour sample, indicative of a significant chemical modification of the ZnO surface.^{46, 54} First indications for this chemical transformation are already discernable after 24 hours of sensitisation, which has been used in previous optical spectroscopy studies: the C1s, Ru3d and Zn2p photo-lines are broadened by ~20% compared to the 2 hour reference sample, and the Ru3d_{5/2} peak exhibits a notable asymmetry and shift to higher binding energies.

Since etching and dissolution of ZnO is governed by the local dye concentration and effective exposure time,^{48, 54} N3-Zn²⁺ agglomerates are expected to form more readily on the outer surface of the ZnO electrode which is in direct contact with the dye bath during sensitisation. In contrast, dye uptake into the bulk of the electrode is governed by slow diffusion of the molecules through the nanoporous ZnO network. Therefore, a sensitisation time of 24 hours might be sufficiently short to inhibit excessive dye-Zn²⁺ complex formation within the bulk of the ZnO electrode, which is compatible with bulk sensitive optical probes. For the surface-sensitive TRXPS experiments reported herein, however, we limit the sensitisation times to 2 hours, which can be considered a reasonable compromise between sufficient dye chemisorption at the outer surface of the ZnO electrode and minimal chemical modification of the surface of the ZnO film.

Setup and X-ray/ laser synchronisation

Generally, pump lasers used in synchrotron-based laser-pump/X-ray probe experiments operate at significantly lower pulse repetition rates than the X-ray light sources. This mismatch renders the traditional pump-probe approach that is marked by a single, tunable delay between the pump- and probe-pulses challenging. The laser is frequently synchronised with a specific electron bunch, employing special, low repetition rate storage ring fill patterns and/or mechanical and electronic gates to discriminate all signals but those associated with a single X-ray pulse at the desired pump-probe time delay.⁵⁵⁻⁵⁷ This technique often results in significantly reduced data collection efficiency compared to static X-ray measurements since only a fraction of the available X-ray flux is used in the experiment. Additionally, it exposes the sample to significantly more, potentially damaging X-ray flux than required to acquire the X-ray spectra. However, the scheme provides the best possible time resolution, ultimately defined by the synchrotron pulse duration. In a different approach, fast time-resolving detectors are used to register and sort the data produced by all X-ray pulses in time, thereby 'passively' monitoring the pump-probe

delay.^{34, 58} The time resolution in this time-tagging approach is usually limited to a few nanoseconds and dominated by the characteristics of the spectrometers and detectors.

The TRXPS setup presented here is schematically shown in Fig. 3. It combines aspects of both detection principles resulting in enhanced data acquisition efficiency, reduced target damage, and an X-ray pulse duration limited time resolution. The experiments are carried out at beamline 11.0.2 of the ALS using the ambient-pressure photoemission spectroscopy end-station.⁵⁹ A hemispherical electron analyser at this end-station is equipped with a two-dimensional delay line⁶⁰ (DLD) that records the arrival time and hit position of all photoelectrons reaching the detector. The hit position along the dispersive plane of the analyser provides the kinetic energy of every electron while the time of arrival marks the pump-probe delay. The kinetic energy window that can be imaged in this snap-shot mode is ~13% of the analyser pass energy. A pass energy of 150 eV was found to provide a good compromise between spectral resolution and total kinetic energy range for the TRXPS experiments described herein.

The overall accuracy for resolving different arrival times of electrons with the same kinetic energy is limited by their time-of-flight spread caused by different trajectories through the lens system and hemisphere of the XPS analyser. In particular, the latter is generally a function of the pass energy and lens mode.^{34, 58} For the setup shown in Fig. 3, we recently demonstrated a time resolution of 860 ps.⁶¹

The laser system employed (Time Bandwidth Products DUETTO) produces 10 ps pulses with selectable wavelengths (1064 nm, 532 nm, 355 nm) and adjustable repetition rates ranging from single shots up to ~8 MHz. All experiments discussed in the following made use of the 532 nm output. Synchronisation between the laser pulses and the X-ray pulse train is achieved using the 500 MHz RF master clock of the ALS as a reference signal (Fig. 3). This master clock has a fixed phase relationship with the RF signal that defines the electron bunch pattern in the storage ring and is therefore intrinsically synchronised with the emitted X-ray pulse train. The laser oscillator operates at 83 MHz and can be locked to the reference signal with a phase-lock-loop provided by a commercial clock synchroniser unit (Time Bandwidth Products, CLX-1100). A 1/6 frequency divider is used to convert the 500 MHz master clock signal into an 83 MHz reference signal. A pulse picker routes a fraction of the oscillator pulses into the laser amplifier. The trigger signal for the pulse picker is derived from the same reference as the synchronisation signal for the oscillator and processed by a programmable frequency divider (PFD) to select pulses at a user-defined repetition rate. This signal also triggers the data acquisition of the DLD.

The time delay between the laser pulses and the ALS X-ray pulse train is coarsely adjusted in steps of 12 ns (oscillator pulse spacing) by using a delay generator (DG) installed in the pulse picker synchronisation branch. The laser/X-ray time delay is fine-tuned via an electronic phase shifter in steps of 5 ps (total range 5 ns). The optical pump pulse remains synchronised to individual X-ray pulses in the ALS pulse train with picosecond precision over periods up to several days.

During multi-bunch operation of the ALS, 296 of the available 328 storage ring fill pattern buckets contain electron bunches separated by ~2 ns and with a round-trip time of ~656 ns. Additionally, a more intense, isolated electron bunch ('camshaft') is placed in a ca. 60-70 ns wide gap of the fill pattern. As illustrated in

Fig. 3, this enables efficient laser-pump multiple X-ray probe measurements that simultaneously monitor pico- to nanosecond time scales. In the ALS two-bunch mode, only one pair of intense electron bunches with a pulse separation of 328 ns is injected in the ring. The resultant time structure of the emitted X-rays is especially advantageous for the characterisation of dynamics proceeding on a picosecond time scale.

Laser and X-ray beam characterisation

The ability to achieve and monitor spatiotemporal overlap between the X-ray and laser beams at the location of the sample is an important prerequisite for any pump-probe experiment. In the TRXPS setup described herein, spatial overlap is accomplished by recording knife-edge scans of the X-ray and the laser beam using the sharply defined sensitive area of a photodiode. The diode is mounted on the same motorized XYZ-manipulator as the samples and scanned across both X-ray and laser beams. Typical results obtained for the horizontal and vertical scan directions in the sample plane are summarized in Figs. 4A and B, respectively. The laser and X-ray beams are combined using an annular mirror inside the vacuum chamber and directed to the sample surface at an angle of incidence of $\sim 45^\circ$. The laser beam pointing is fine-tuned by a piezo-actuator (Newport Picomotor) controlled mirror mount outside the vacuum chamber. The centroids of the X-ray and laser beam profiles are overlapped in both dimensions by iterative scanning and tuning of the piezo-actuator. Spatial pump-probe overlap can be adjusted with a precision better than $20 \mu\text{m}$ within minutes.

The measurements in Fig. 4 indicate X-ray spot size diameters $< 100 \mu\text{m}$ (FWHM) in both the vertical and horizontal direction. In order to ensure uniform optical excitation density across the area probed by the X-ray beam, the laser spot size on the target was deliberately chosen to be significantly larger than the X-ray spot size, as illustrated by the $\sim 250 \times 180 \mu\text{m}^2$ (FWHM) optical beam profile at the sample surface. Note that all values include the projection-induced broadening in the horizontal beam dimensions caused by the $\sim 45^\circ$ incidence angle. For the given spot size, the available laser output power at 532 nm is sufficiently high to enable pump-probe experiments with repetition rates of up to 1 MHz at pump fluences of several mJ/cm^2 (Fig. 4D).

Temporal overlap and time resolution

The coarse relative timing of the laser pulses with respect to the ALS X-ray pulse train is adjusted to within $\pm 0.3 \text{ ns}$ by displaying the time traces of an avalanche photodiode mounted on the sample holder on a 1 GHz bandwidth oscilloscope. The timing stability is continuously monitored by observing the leakage through one of the laser steering mirrors on an oscilloscope that is triggered by the ALS bunch-marker clock. The pump-probe temporal overlap is tuned in the picosecond range by performing an X-ray/laser cross-correlation using the transient surface photo-voltage (SPV) effect of a semiconductor sample.

The position of the Fermi level at semiconductor surfaces can be pinned by surface- and impurity-states near the middle of the band gap.⁶² The resultant charge transfer to the surface gives rise to a space charge region (typically $\sim 100 \text{ nm}$ deep) causing a characteristic downward (upward) bending of all energy levels for p-type

(n-type) semiconductors toward the surface. Laser illumination with photon energies exceeding the band gap generates electron-hole pairs that partly compensate the electric field in the space charge layer. This leads to a transient flattening of all energy bands near the surface depending on the recombination dynamics of the electron-hole pairs inside the material. The SPV effect therefore manifests itself as a rigid, time-dependent shift of the entire photoelectron spectrum to lower (higher) binding energies for p-doped (n-doped) materials. The build-up of the transient SPV response is governed by the diffusion of photo-generated minority carriers in the space charge region to the semiconductor surface,⁶² which usually proceeds on a sub-picosecond time scale.³² The SPV effect therefore represents a suitable benchmark to measure the time resolution in TRXPS experiments.

We have investigated the SPV dynamics in thin (~3 μm) ZnO films grown on p-doped Si(100), which also served as substrates for the N3 dye molecules in the TRXPS experiments discussed later in this article. To identify the dominant time scale in the SPV response from the ZnO/Si samples, TRXPS in the time-tagging only mode, i.e., without any synchronisation between the laser and X-ray pulses, have been performed. As demonstrated in Fig. 5A, this allows the efficient measurement of transients in a time window only limited by the laser repetition rate (~102 kHz in this experiment). The measured deviation of the Zn3d binding energy relative to a laser-off reference spectrum is plotted as a function of the time delay between the optical pump pulse and the 850 eV X-ray probe pulse for different laser fluences. The sudden drop in the Zn3d binding energy observed around $\Delta t = 0$ signals the arrival of the laser pulse at the sample surface. The subsequent relaxation of the SPV shift lasts for several microseconds and is strongly influenced by the pump fluence. For laser fluences $> 20 \mu\text{J}/\text{cm}^2$, the Zn3d line position does not recover to the laser-off situation within the laser pump period (~10 μs). This accumulated SPV contribution is observed as a constant binding energy offset at negative pump-probe delays. We note that no SPV effect was observed for laser fluences up to $10 \text{ mJ}/\text{cm}^2$ in ZnO films deposited on stainless steel substrates (green curve in Fig. 5A). Thus, the SPV dynamics probed by Zn3d TRXPS originates exclusively from laser-excited electron-hole pairs generated in the space charge region at the ZnO/Si interface. This also explains the transient drop (instead of an increase) in the observed Zn3d binding energy, which is not expected from the n-doped ZnO film but from the p-doped Si substrate.³¹ The possibility to monitor electronic dynamics at buried interfaces by TRXPS has been reported before by the Wurth group for BaF₂/Si interfaces.⁶³ All traces shown in Fig. 5A have been acquired during ALS two-bunch operation with a data acquisition time of 15 min per trace.

The picosecond time-resolved drop of the effective Zn3d binding energy near $\Delta t = 0$ is presented in Fig. 5B. For this measurement, the laser was synchronised to the X-ray pulse train and the electronic phase shifter of the oscillator timing electronics (Fig. 3) was used to scan the delay of the laser pump pulse with respect to the ALS probe pulse. A fit of the SPV response to a Gaussian error function reveals a ~70 ps TRXPS time resolution (FWHM), which is in agreement with the previously reported ALS bunch length.³³

To benchmark the performance of the TRXPS apparatus compared to existing setups, additional picosecond time-resolved SPV experiments on p-doped GaAs(100) have been carried out. The SPV effect in this material has been extensively studied and is more pronounced compared to other semiconductor materials with band gaps compatible with the pump laser photon energy (2.33 eV). Figure 6 summarises the

change in the Ga3d binding energy as a function of laser-pump/ X-ray-probe (450 eV) delay. The data was recorded within 50 min acquisition time (integration time ~ 80 s per pump probe step) during ALS two-bunch operating mode with a laser repetition rate of ~500 kHz and a laser fluence of 10 nJ/cm², which is safely below the photo-chemical decomposition threshold of GaAs.⁶⁴

The rapid build-up of the SPV effect is followed by a much slower decay of the SPV shift proceeding on a nanosecond time scale. The relaxation dynamics are governed by two different channels: a fast process leading to a reduction of the SPV shift by 40% within approximately 200 ps after laser excitation, and a second component responsible for a slower decrease over several nanoseconds. A bi-exponential decay model fitted to the data (red line in Fig. 6) yields time constants of 80±30 ps and 2.3±0.4 ns, respectively, for the fast and slowly decaying components. Such biphasic relaxation behaviour of the SPV effect has previously been observed in GaAs and was attributed to tunnelling and thermionic recombination of the photo-excited charge carriers on fast and slow time scales, respectively.^{36, 65, 66} We note that photoelectron spectra recorded before the laser pulse reaches the surface are still shifted by ca. 50 meV to lower binding energies compared to spectra recorded without any laser illumination. The transient SPV effect has therefore not fully decayed within the time scale of the experiment, i.e. the time elapsed between two laser pulses (1.7 μs). This suggests the existence of (at least) a third relaxation channel with a time constant in the microsecond or even millisecond range.⁶⁶

The time-resolved SPV measurements presented above highlight the capability of the TRXPS setup to capture electron-hole recombination dynamics on the pico- to microsecond time scale at semiconductor surfaces and buried interfaces by laser-pump/X-ray probe photoelectron spectroscopy with an overall time resolution only limited by the ALS electron bunch duration.

Results

The TRXPS experiments presented here concentrate on the binding energy region comprising the C1s peaks and the Ru3d doublet. This provides, in principle, simultaneous sensitivity to charge dynamics affecting the metal centre and the aromatic ligands of the dye molecule (Fig. 1).

Typical C1s/Ru3d TRXPS data of N3-sensitised films of ZnO nanocrystals obtained during ALS multi- and two-bunch operating mode are summarised in Fig. 7. For these measurements, the laser system was operated at a repetition rate of ~102 kHz, which enables temporal overlap of the laser pulses with one out of 15 camshaft pulses in multi-bunch or one out of 30 camshaft pulses in two-bunch operating mode. The laser fluence was set to 10 mJ/cm² and the sample was continuously scanned at a speed of 120 μm/s to minimise laser and X-ray induced beam damage.

Figs. 7A and B show false-colour representations of the acquired TRXPS spectra. Each slice of the false-colour map along the (horizontal) energy axis corresponds to an XPS spectrum recorded at a well-defined time delay after laser excitation. Projections onto the time axis reveal the characteristic multi- and two-bunch fill pattern of the ALS in Figs. 7A and B, respectively. Note that the individual pulses in the multi-bunch sections are not fully resolved due to the ~5 ns resolution of the time-tagging technique, which was determined by the pass energy and lens mode

employed in this particular experiment. It is important to note, however, that this only represents the time resolution for the overlapping signals in the multi-bunch probe regions, whereas signals associated with the isolated camshaft pulses are still recorded with the bunch-length limited time-resolution of 70 ps.

5 For the two-bunch data set in Fig. 7B, the timing electronics of the setup were adjusted such that the laser pump pulse arrived at the sample surface 30 ps before the second camshaft pulse within the time span recorded by the detector. The relative timing of the laser and X-ray pulses was calibrated by performing an SPV-based cross-correlation immediately before the measurement (see Fig. 5B). XPS
10 spectra recorded ~ 328 ns before (blue) and 30 ± 5 ps after (red) laser excitation are compared in Fig. 7C. The laser-affected spectrum exhibits a pronounced ~ 450 meV shift of both the C1s and the Ru3d_{5/2} lines to higher binding energies. This rigid shift of the entire photoelectron spectrum is ascribed to an SPV effect in the substrate. Signatures of changes in the C1s and Ru line shapes, which are expected to contain
15 information on the electron dynamics at the N3/ZnO interface, are obviously more subtle and require a more detailed analysis. In the following, we base our investigation of laser-induced line-shape variations in the TRXPS spectra exclusively on data recorded during two-bunch operation, since the multi-bunch TRXPS experiments were partly affected by detector saturation. We note, however,
20 that reliable information on the SPV dynamics could nevertheless be extracted from both types of data.

In Fig. 8 we contrast TRXPS spectra acquired at time delays of $\Delta t = 30$ ps (A) and $\Delta t = 30$ ps + 328 ns (C) to a laser-off reference spectrum ($\Delta t = 30$ ps – 328 ns). For accurate comparison of the line shapes, the SPV effect of the laser-on spectra has
25 been corrected by shifting the spectra numerically along the binding energy axis to minimize the squared sum of residuals with the reference spectrum. Whereas the line shape of the spectrum taken at $\Delta t = 30$ ps + 328 ns and the laser-off reference are indistinguishable within the signal-to-noise of the measurement (Figs. 8C and D), distinct laser-induced changes are observed at $\Delta t = 30$ ps (Figs. 8A and B):
30 intensities near the C1s pyridine and the Ru3d_{5/2} peak centres are reduced, accompanied by intensity enhancements in the regions between peaks. This can be seen more clearly in the difference spectra shown in Fig. 8B and D. At $\Delta t = 30$ ps, there are minima at ~ 281 eV and ~ 285 eV with corresponding maxima near ~ 283 eV and ~ 287 eV. Compared to this, no pronounced correlations are observed in the
35 spectral difference at $\Delta t = 30$ ps + 328 ns.

Figure 9 summarises the overall temporal evolution of the SPV response of the N3/ZnO samples. The transient was obtained by combining data sets acquired during different ALS operating modes and with different data acquisition schemes. The amplitude of the SPV rises to almost 500 meV within the time resolution of the
40 experiments and is followed by a rapid decay to 40% within only a few nanoseconds. However, the complete SPV relaxation involves several hundreds of nanoseconds. Note that the curves have a vertical offset of ~ 400 meV due to the transient SPV effect at the ZnO/Si interface discussed above, which does not relax on the time scale of the laser pump period.

45

Discussion

In N3, photon absorption proceeds via excitation of a singlet metal-to-ligand charge transfer ($^1\text{MLCT}$) state. Subsequent depopulation of the initially excited state may occur, in principle, via direct (<100 fs) electron injection into the substrate or via intramolecular relaxation to the metastable $^3\text{MLCT}$ triplet state, followed by much slower electron injection (~10-100 ps).^{4, 7} The relative importance of both channels may depend on the specific dye-semiconductor system and has long been a matter of debate.^{4, 6, 7, 20, 67} Since the HOMO of N3 is predominantly located at the metal centre and the thiocyanate groups of the dye, whereas the LUMO resides mostly on the pyridine ligands that bond the molecule to the semiconductor, the ruthenium photoemission lines are expected to carry information of the transient charge redistribution within the dye.⁵² In either relaxation channel, the light-induced charge redistribution is intuitively expected to manifest itself in an increase of binding energies of the ruthenium core levels because of the reduced electron density around the metal centre that screens the ruthenium core holes. This effect has indeed been observed for isolated N3 molecules in solution²¹ and in a recent femtosecond TRXPS experiment on N3/ZnO at the Linac Coherent Light Source (LCLS).⁴¹

As illustrated in Figs. 8A and B, the difference spectrum at $\Delta t = 30$ ps can indeed be qualitatively rationalised in terms of a laser-induced shift of the Ru3d doublet by $\Delta\text{BE} \sim 2$ eV to higher binding energies for a fraction $F \sim 10\%$ of the N3 molecules. A corresponding fit is indicated as a green solid line. We note that F and ΔBE are the only free parameters in this model function, since the ground-state photoemission line shape can be extracted from the isolated Ru3d_{5/2} emission line in the laser-off spectrum, and the well-known Ru3d spin-orbit splitting and intensity ratio.⁵¹

While ultrafast optical spectroscopy studies have shown that electron injection in N3/ZnO is dominated by “slow” electron transfer channels with time constants in the range of a few to hundreds of picoseconds (compared to, e.g., ≤ 100 fs in N3/TiO₂), the microscopic origin for this behaviour is not fully understood.^{8, 40, 67-69} Two competing descriptions for the charge injection process have been proposed: (i) an intermediate-interface-state model^{40, 69-72} and (ii) a two-state injection model.^{8, 39, 67, 73, 74} In (i), optical excitation of the dye results in the formation of an electron-cation complex that temporarily binds the injected electron to the interface on a time scale of <5 ps before it subsequently decays within 10-150 ps to generate mobile charge carriers in the semiconductor conduction band.^{8, 67, 68, 74} In this case, the dielectric properties of the substrate are expected to have a major impact on the interfacial electron dynamics.⁸ In (ii), unfavourable electronic coupling between the dye and the ZnO substrate is suggested, leading to reduced injection efficiency due to an increased competition with intramolecular relaxation. In this case, the majority of N3 molecules initially excited in the singlet metal-to-ligand charge transfer state $^1\text{MLCT}$ undergo relaxation to the metastable $^3\text{MLCT}$ triplet state that is expected to inject on a much slower time scale (10-100 ps).^{40, 69}

Evidently, the two scenarios are characterised by distinctly different spatial distributions of the excited electronic charge during the first tens of picoseconds after excitation. In (i) it would be transferred to the semiconductor but still localised at the interface at the beginning of the injection process, whereas it would initially reside on the dye in scenario (ii). The exact magnitude and time evolution of the TRXPS Ru3d binding energy shift may therefore provide valuable insight into the dominant injection mechanisms. Recent DFT calculations indicate that the two

scenarios may lead to Ru3d chemical shifts that differ by approximately 1 eV.⁷⁵ Unfortunately, as indicated by the green shaded area in Fig. 8B, the signal-to-noise level in the current measurements does not permit an identification of the transient chemical shift at $\Delta t = 30$ ps within this level of precision. However, modest improvements of the experiment are expected to enable future investigations that will provide this information.

Apparently, the marked minimum at ~ 285 eV in the $\Delta t = 30$ ps difference spectrum is not well reproduced by the Ru3d model function described above. This might indicate that transient changes in one or more C1s photo-lines contribute to the differential laser-on/laser-off effect. In this respect it is noteworthy that a recent stationary high-resolution XPS study of N3 demonstrated that the most dominant C1s peak is composed of two different components corresponding to carbon atoms in two different chemical environments within the N3 pyridine groups.⁴³ The high binding energy component was assigned to the two carbon atoms bonded to the nitrogen atom, whereas the lower binding energy component was ascribed to the three carbon atoms in the pyridine ring that are in closer proximity to the carboxylic acid group. The binding energies of the two components differ by 1 eV. These findings are compatible with the slightly asymmetric C1s pyridine line shape in Fig. 8A and C. The additional differences observed at ~ 285 eV binding energy may therefore indicate a temporal increase of the C1s binding energies in carbon atoms that are located closer to the carboxylic acid groups than the nitrogen atoms (Fig. 1A). In addition, a potential contribution from the (spectrally unresolved) C1s emission originating from the thiocyanate groups has to be considered.

Even though the electron injection process in N3/ZnO is essentially completed after ~ 200 ps,⁸ one may still expect signatures of the oxidised N3 dyes in the $\Delta t = 30$ ps + 328 ns TRXPS spectrum, unless the dye molecules have been completely reduced by charge recombination processes. The absence of evident correlations in the difference spectrum in Fig. 8D therefore suggests that ~ 300 ns after laser excitation, the majority of the initially excited N3 molecules have already returned to the neutral ground state by back-electron transfer from the ZnO substrate.

Reported time scales for relaxation processes at dye-semiconductor interfaces range from a few picoseconds to several milliseconds.^{2, 6, 18, 23} In this respect the question arises whether the N3/ZnO SPV transient in Fig. 9 contains information on the interfacial charge recombination dynamics. Thus, it is important to identify the exact origin of the SPV effect in this system. For laser fluences > 1 mJ/cm², the SPV effect induced in the ZnO/p-Si support of the N3 molecules is completely saturated on a microsecond time scale (see Fig. 5A),⁶¹ and can therefore not contribute to the nanosecond dynamics apparent in Fig. 9. The saturated SPV effect of the ZnO/p-Si is indeed observed as a constant ~ 400 meV shift of all TRXPS spectra to higher binding energy when the laser beam is blocked. Therefore, the n-type behaviour of the SPV transient in Fig. 9 must originate from the ZnO nanoparticles and/or the N3 molecules, and might be influenced by electron exchange across the interface.

The direct band gap of ZnO is ~ 3.3 eV³ and significantly exceeds the laser photon energy in our experiment (2.33 eV). In order for direct ZnO photo-excitation to be the origin of the observed SPV dynamics, one would have to invoke excitation into or from band-gap states (a nonlinear response of the semiconductor is unlikely at the applied pump laser fluence). However, this effect can be ruled out since no SPV signature is observed in ZnO/stainless steel samples for laser fluences up to 10 mJ/cm² (green trace in Fig. 5A). Since ZnO films are intrinsically n-doped (due to

interstitial Zn atoms or oxygen vacancies)⁷⁶ the SPV transient in Fig. 9 may result from electron injection from the dye adsorbate into the ZnO substrate, which would have a similar effect as electron-hole pair creation directly in the substrate by super-bandgap excitation. For the n-type semiconductor ZnO, this would lead to transient lowering of the band edges near the surface (increased binding energies) during the electron injection process, followed by an SPV relaxation (decreasing binding energies) governed by the time scale of the charge recombination processes that neutralise the N3 molecules at the surface. This picture is consistent with the SPV behaviour in Fig. 9. We note that the N3/ZnO SPV relaxation dynamics can only be described satisfactorily using (at least) a bi-exponential decay model, which suggests contributions from recombination times of ~10 ns and ~100 ns (red dashed line in Fig. 9). These time scales are well within the range of recombination times reported in previous optical studies for N3/ZnO.²³

Future studies will shed more light on the processes and mechanisms underlying the transient changes in the Ru3d/C1s line shapes and the substrate SPV response described herein. In particular, a more complete picture will be achieved by performing TRXPS experiments addressing the O1s, S2p and N1s core levels. Experiments involving the nitrogen atoms will be particularly interesting, since the thiocyanate- and pyridine-related emission lines can be distinguished in the N1s XPS spectrum and the N3 HOMO and LUMO have significantly different amplitudes on the corresponding atomic positions.⁵²

Conclusion and outlook

An experimental setup for synchrotron-based picosecond time-resolved X-ray photoelectron spectroscopy (TRXPS) studies is presented. A unique combination of high temporal resolution and data collection efficiency is achieved by implementing both a picosecond laser/X-ray synchronisation scheme and a nanosecond time-resolved time-stamping technique. The potential of the method is demonstrated by monitoring light-induced electronic dynamics at the interface between N3 dye-molecules and a nanostructured ZnO semiconductor substrate. Transient changes in the C1s/Ru3d TRXPS line shapes are observed, which are indicative of a change in oxidation state of the Ru metal centre of the dye molecule 30 ps after laser excitation. Further studies are required to determine a comprehensive picture of the transient valence electron configurations that are reflected in the time-dependent XPS line shapes, and to explore their correlation with the macroscopic surface photovoltage response observed in this system.

Detailed static XPS studies suggest that the N3 sensitisation procedure of ZnO has to be adapted to the specific spectroscopic method by which the dynamics at the dye-semiconductor interface are probed in order to avoid a detrimental impact of chemical modifications.

Although the TRXPS experiments presented here have been performed under vacuum conditions, the ambient-pressure capability of the employed hemispherical analyser and beamline enables TRXPS studies with background pressures up to 10 Torr. We envision that this will enable *in situ* studies of the interplay between charge dynamics and solvent/electrolyte-induced modification of the dye-substrate interaction, which is believed to significantly influence the performance of dye-sensitised solar cells. The TRXPS experiments will be complemented by time-resolved X-ray absorption measurements based on Auger or partial electron yields

recorded with the same experimental setup. These measurements will provide additional, site-specific information on the time evolution of the unoccupied valence states of the system. Combined, these methods have the potential to provide comprehensive, atomic site-specific real-time insight into interfacial photovoltaic and photocatalytic reaction dynamics approaching application-like conditions.

Acknowledgements

This work was supported by the U.S. Department of Energy, Office of Basic Energy Sciences, Chemical Sciences, Geosciences and Biosciences Division, through
10 Contract No. DE-AC02-05CH11231. O.G. was supported by the Department of Energy Office of Science Early Career Research Program. J.Z.Z. is grateful for support by the Basic Energy Sciences Division of the US DOE (DE-FG02-ER46232). We appreciate the excellent support provided by the staff of the Advanced Light Source.

15

20

Figures captions

Fig. 1 Illustration of the application of TRXPS to study electron dynamics at the prototypical dye-semiconductor interface N3/ZnO. The relevant processes are shown schematically (A) in real-space and (B) in the energy domain.

Fig. 2 Characterisation of N3-sensitised ZnO electrodes with stationary XPS. (A) XPS spectrum of an N3/ZnO electrode recorded with $h\nu = 850$ eV photon energy after 2 hours of sensitisation. Detailed views of the N1s, C1s and S2p core-level emission lines are shown as insets. (B) Comparison of XPS spectra in the region of the C1s and Ru3d photoemission lines obtained from ZnO electrodes after 2 hours, 24 hours and 6 days of N3 sensitisation. The spectra were recorded with $h\nu = 490$ eV to enhance the surface sensitivity. (C) Photographs of electrodes with different sensitisation times (from bottom to top): 2 hours, 24 hours, and 6 days. (D) Zn2p_{3/2} photoemission lines of N3-sensitised electrodes produced with different sensitisation times ($h\nu = 1250$ eV).

Fig. 3 Setup for picosecond time-resolved laser-pump/X-ray photoemission probe spectroscopy at the Advanced Light Source (ALS). Key components of the electronic laser/X-ray synchronisation scheme are indicated (DG = delay generator; PFD = programmable frequency divider). See text for details.

Fig. 4 Spatial profiles of the laser and X-ray beams, which are overlapped at the sample surface inside the vacuum chamber. Horizontal (A) and vertical (B) beam profiles are obtained by scanning a large-area photodiode mounted on the sample holder through the beams. Solid lines are Gaussian fits to the data. The beam paths employing a perforated mirror (PM) as a beam combiner and the measurement geometry with the photodiode (PD) and the hemispherical electron analyser (HEA) are illustrated in C. The maximum fluence that can be delivered to the sample by the employed laser system based on the spot size determined in A and B is shown in D as a function of the laser repetition rate.

Fig. 5 Transient surface photo-voltage (SPV) dynamics at the ZnO/p-Si(100) interface probed by TRXPS. A Evolution of the Zn3d line position as a function of pump-probe delay for different laser pulse fluences. The data was acquired using the time tagging method without active laser/X-ray synchronisation. B SPV shifts extracted from picosecond time-resolved photoemission spectra near the temporal overlap between the X-ray-probe and the laser-pump pulse ($17 \mu\text{J}/\text{cm}^2$) after laser/X-ray synchronisation. Fitting to a Gaussian error function (red solid line) yields the time resolution of the TRXPS experiment (~ 70 ps).

Fig. 6 TRXPS from p-doped GaAs(100). Blue circles show the SPV-induced reduction of the Ga3d core-level binding energy measured relative to the peak position in a laser-off spectrum (inset) as a function of pump-probe delay. The fit (red solid line) describes a step-like binding energy drop followed by a bi-exponential recovery convoluted with the Gaussian instrument response function.

Fig. 7 C1s/Ru3d TRXPS maps acquired from N3/ZnO during the (A) multi- and (B) two-bunch operation modes of the ALS. Photoelectron spectra as a function of laser-pump/X-ray-probe time delay are displayed in a false colour representation – with a projection of the data onto the time axis shown on the left side. The laser pulse excites the sample surface 120 ps before the first camshaft X-ray pulse (A) and 30 ps before the second X-ray pulse (B) in the chosen detection time window. C Comparison of photoelectron spectra recorded during ALS two-bunch mode. The spectrum of the camshaft arriving $\Delta t = 30$ ps after the laser pulse at the sample (red) is shifted to higher binding energies with respect to the spectrum of the camshaft that arrives 328 ns before laser excitation (blue).

Fig. 8 Evidence for laser-induced TRXPS line-shape variations. **A** Comparison of a laser-off Cls/Ru3d photoemission spectrum ($\Delta t = 30$ ps - 328 ns, blue) to a spectrum recorded at a pump-probe delay of 30 ps (red). The laser-on spectrum was shifted numerically to compensate for the SPV effect. The insets highlight the spectral region near the Ru3d_{5/2} emission line. **B** Difference spectrum obtained by subtracting the laser-off reference from the SPV-corrected laser-on spectrum. The fit result (green solid line) is based on a model that describes the entire laser-on/laser-off difference by a shift ΔBE of the Ru3d doublet in a fraction $F \approx 10\%$ of the probed dye molecules to ~ 2 eV higher binding energies (indicated by green arrows in A). The green shaded area highlights the array of difference spectra predicted by this model for the parameter range $\Delta BE = 1.5 - 3$ eV and $F = 10 - 25\%$. See text for details. **C** and **D** show the corresponding analysis of a photoemission spectrum recorded at a pump-probe delay of $\Delta t = 30$ ps + 328 ns. No systematic differences between the laser-on and laser-off spectra are observed in this case.

Fig. 9 Time evolution of the N3-induced SPV in the N3/ZnO/Si system. The SPV shift is quantified by minimizing the spectral difference with a laser-off reference spectrum. The change in binding energy is given relative to a spectrum recorded without any laser illumination. Colour coding of the circles refer to results obtained for different ALS operating modes and analyser configurations. The red dashed line is a bi-exponential decay approximation of the observed SPV dynamics.

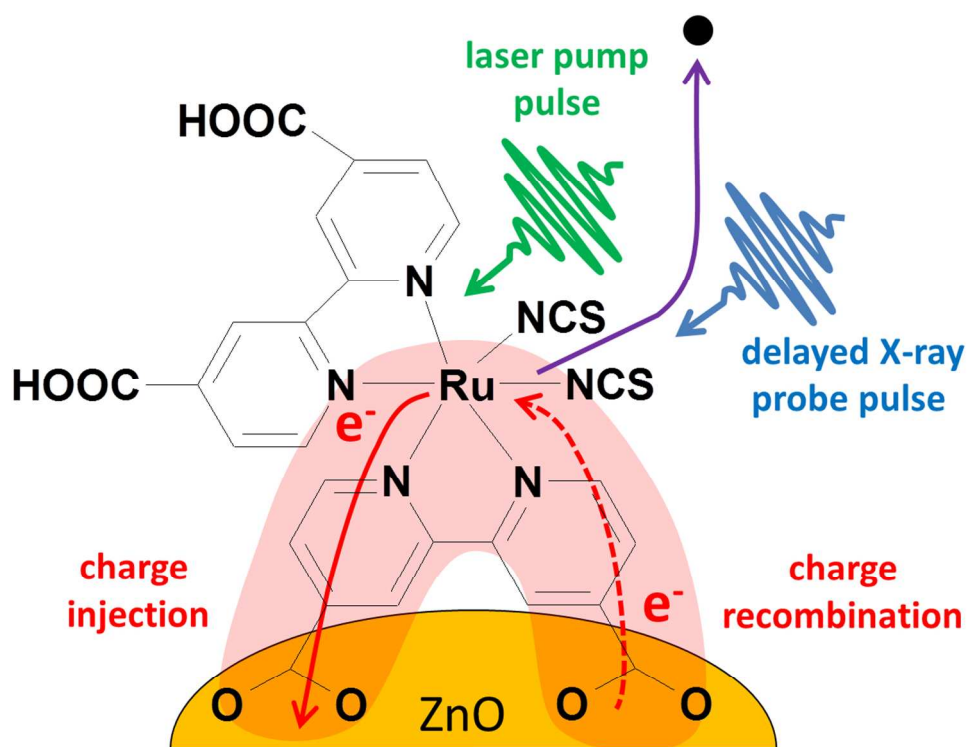
20

References

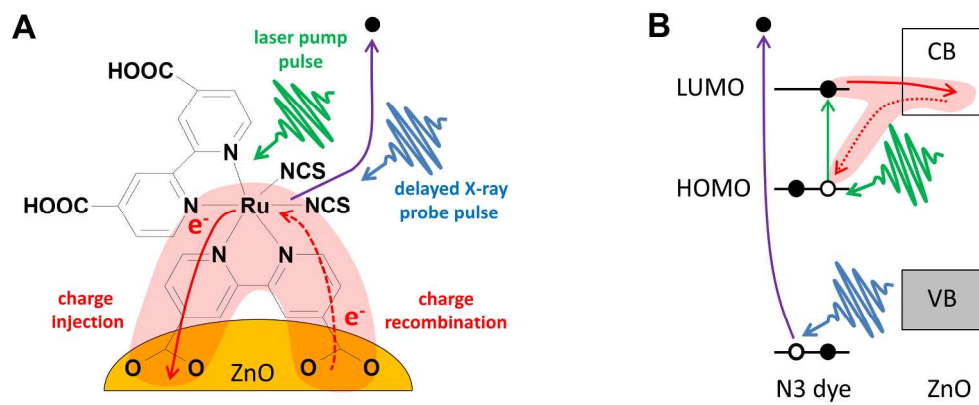
1. M. Grätzel, *Journal of Photochemistry and Photobiology C: Photochemistry Reviews*, 2003, 4, 145-153.
2. Y. Tachibana, S. A. Haque, I. P. Mercer, J. R. Durrant and D. R. Klug, *The Journal of Physical Chemistry B*, 2000, 104, 1198-1205.
3. S. B. Rana, A. Singh and S. Singh, *International Journal of Nanoelectronics & Materials*, 2013, 6, 45-57.
4. N. A. Anderson, X. Ai and T. Lian, *The Journal of Physical Chemistry B*, 2003, 107, 14414-14421.
5. G. Benkő, J. Kallioinen, J. E. I. Korppi-Tommola, A. P. Yartsev and V. Sundström, *Journal of the American Chemical Society*, 2001, 124, 489-493.
6. R. Katoh, A. Furube, A. V. Barzykin, H. Arakawa and M. Tachiya, *Coordination Chemistry Reviews*, 2004, 248, 1195-1213.
7. N. A. Anderson and T. Lian, *Annual review of physical chemistry*, 2005, 56, 491-519.
8. H. Němec, J. Rochford, O. Taratula, E. Galoppini, P. Kužel, T. Polívka, a. Yartsev and V. Sundström, *Physical Review Letters*, 2010, 104, 197401-197401.
9. E. Goulielmakis, M. Schultze, M. Hofstetter, V. S. Yakovlev, J. Gagnon, M. Uiberacker, A. L. Aquila, E. M. Gullikson, D. T. Attwood, R. Kienberger, F. Krausz and U. Kleineberg, *Science*, 2008, 320, 1614-1617.
10. E. Magerl, S. Neppel, A. L. Cavalieri, E. M. Bothschafter, M. Stanislowski, T. Uphues, M. Hofstetter, U. Kleineberg, J. V. Barth, D. Menzel, F. Krausz, R. Ernstorfer, R. Kienberger and P. Feulner, *Rev. Sci. Instr.*, 2011, 82, 63104-63104.
11. A. D. Shiner, C. Trallero-Herrero, N. Kajumba, H. C. Bandulet, D. Comtois, F. Légaré, M. Giguère, J. C. Kieffer, P. B. Corkum and D. M. Villeneuve, *Physical Review Letters*, 2009, 103, 073902.
12. P. Emma *et al.*, *Nat Photon*, 2010, 4, 641-647.
13. W. Ackermann *et al.*, *Nat Photon*, 2007, 1, 336-342.
14. T. Ishikawa *et al.*, *Nat Photon*, 2012, 6, 540-544.
15. A. Pietzsch, A. Föhlisch, M. Beye, M. Deppe, F. Hennies, M. Nagasono, E. Suljoti, W. Wurth, C. Gahl, K. Döbrich and A. Melnikov, *New Journal of Physics*, 2008, 10, 033004.

16. L. Wang, W. Chen and A. T. S. Wee, *Surface Science Reports*, 2008, 63, 465-486.
17. M. Weston, A. J. Britton and J. N. O'Shea, *The Journal of Chemical Physics*, 2011, 134, 054705.
18. A. Listorti, B. O'Regan and J. R. Durrant, *Chemistry of Materials*, 2011, 23, 3381-3399.
- 5 19. J. J. H. Pijpers, R. Ulbricht, S. Derossi, J. N. H. Reek and M. Bonn, *The Journal of Physical Chemistry C*, 2011, 115, 2578-2584.
20. H. Němec, J. Rochford, O. Taratula, E. Galoppini, P. Kužel, T. Polivka, A. Yartsev and V. Sundström, *Physical Review Letters*, 2010, 104, 197401.
21. B. E. Van Kuiken, N. Huse, H. Cho, M. L. Strader, M. S. Lynch, R. W. Schoenlein and M. Khalil, *The Journal of Physical Chemistry Letters*, 2012, 3, 1695-1700.
- 10 22. M. Saes, C. Bressler, R. Abela, D. Grolimund, S. L. Johnson, P. A. Heimann and M. Chergui, *Physical Review Letters*, 2003, 90, 047403.
23. C. Bauer, G. Boschloo, E. Mukhtar and A. Hagfeldt, *The Journal of Physical Chemistry B*, 2001, 105, 5585-5588.
- 15 24. C. Bressler and M. Chergui, *Annual review of physical chemistry*, 2010, 61, 263-282.
25. X. Zhang, G. Smolentsev, J. Guo, K. Attenkofer, C. Kurtz, G. Jennings, J. V. Lockard, A. B. Stickrath and L. X. Chen, *The Journal of Physical Chemistry Letters*, 2011, 2, 628-632.
26. A. Cavalleri, H. H. W. Chong, S. Fourmaux, T. E. Glover, P. A. Heimann, J. C. Kieffer, B. S. Mun, H. A. Padmore and R. W. Schoenlein, *Physical Review B*, 2004, 69, 153106.
- 20 27. R. W. Schoenlein, S. Chattopadhyay, H. H. W. Chong, T. E. Glover, P. A. Heimann, C. V. Shank, A. A. Zholents and M. S. Zolotarev, *Science*, 2000, 287, 2237-2240.
28. C. Stamm, T. Kachel, N. Pontius, R. Mitzner, T. Quast, K. Holldack, S. Khan, C. Lupulescu, E. F. Aziz, M. Wietstruk, H. A. Durr and W. Eberhardt, *Nat Mater*, 2007, 6, 740-743.
- 25 29. M. H. Rittmann-Frank, *Angewandte Chemie (International Edition) accepted*, 2014.
30. S. Hüfner, *Photoelectron Spectroscopy: Principles and Applications*, Springer, 2010.
31. J. P. Long, H. R. Sadeghi, J. C. Rife and M. N. Kabler, *Physical Review Letters*, 1990, 64, 1158-1161.
- 30 32. P. Siffalovic, M. Drescher and U. Heinzmann, *EPL (Europhysics Letters)*, 2002, 60, 924.
33. T. E. Glover, G. D. Ackermann, A. Belkacem, B. Feinberg, P. A. Heimann, Z. Hussain, H. A. Padmore, C. Ray, R. W. Schoenlein and W. F. Steele, *Nuclear Instruments and Methods in Physics Research Section A: Accelerators, Spectrometers, Detectors and Associated Equipment*, 2001, 467-468, Part 2, 1438-1440.
- 35 34. T. Giebel, D. Bröcker, P. Schmidt and W. Widdra, *Review of Scientific Instruments*, 2003, 74, 4620-4624.
35. D. Bröcker, T. Giebel and W. Widdra, *Chemical Physics*, 2004, 299, 247-251.
36. T. Nakanishi, M. Kamada, T. Nishitani, K. Takahashi, S. D. More and S. Tanaka, *Surface Review and Letters*, 2002, 09, 1297-1301.
- 40 37. M. Bauer, C. Lei, K. Read, R. Tobey, J. Gland, M. M. Murnane and H. C. Kapteyn, *Physical Review Letters*, 2001, 87, 025501.
38. H. Dachraoui, M. Michelswirth, P. Siffalovic, P. Bartz, C. Schäfer, B. Schnatwinkel, J. Mattay, W. Pfeiffer, M. Drescher and U. Heinzmann, *Physical Review Letters*, 2011, 106, 107401.
- 45 39. P. Tiwana, P. Docampo, M. B. Johnston, H. J. Snaith and L. M. Herz, *Accounts of chemical research*, 2011, 5, 5158-5166.
40. N. a. Anderson and T. Lian, *Coordination Chemistry Reviews*, 2004, 248, 1231-1246.
41. K. R. Siefertmann *et al.*, Molecular Scale Perspective of Ultrafast Charge Transfer at a Dye-Semiconductor Interface, *submitted*.
- 50 42. M. Weston, A. J. Britton and J. N. O'Shea, *The Journal of Chemical Physics*, 2011, 134, 054705.
43. L. C. Mayor, A. Saywell, G. Magnano, C. J. Satterley, J. Schnadt and J. N. O'Shea, *The Journal of Chemical Physics*, 2009, 130, 164704.
44. E. M. J. Johansson, M. Hedlund, H. Siegbahn and H. Rensmo, *The Journal of Physical Chemistry B*, 2005, 109, 22256-22263.
- 55 45. S. Tanuma, C. J. Powell and D. R. Penn, *Surface and Interface Analysis*, 1991, 17, 927-939.
46. K. Westermark, H. Rensmo, H. Siegbahn, K. Keis, A. Hagfeldt, L. Ojamäe and P. Persson, *The Journal of Physical Chemistry B*, 2002, 106, 10102-10107.
- 60 47. K. Keis, J. Lindgren, S.-E. Lindquist and A. Hagfeldt, *Langmuir*, 2000, 16, 4688-4694.

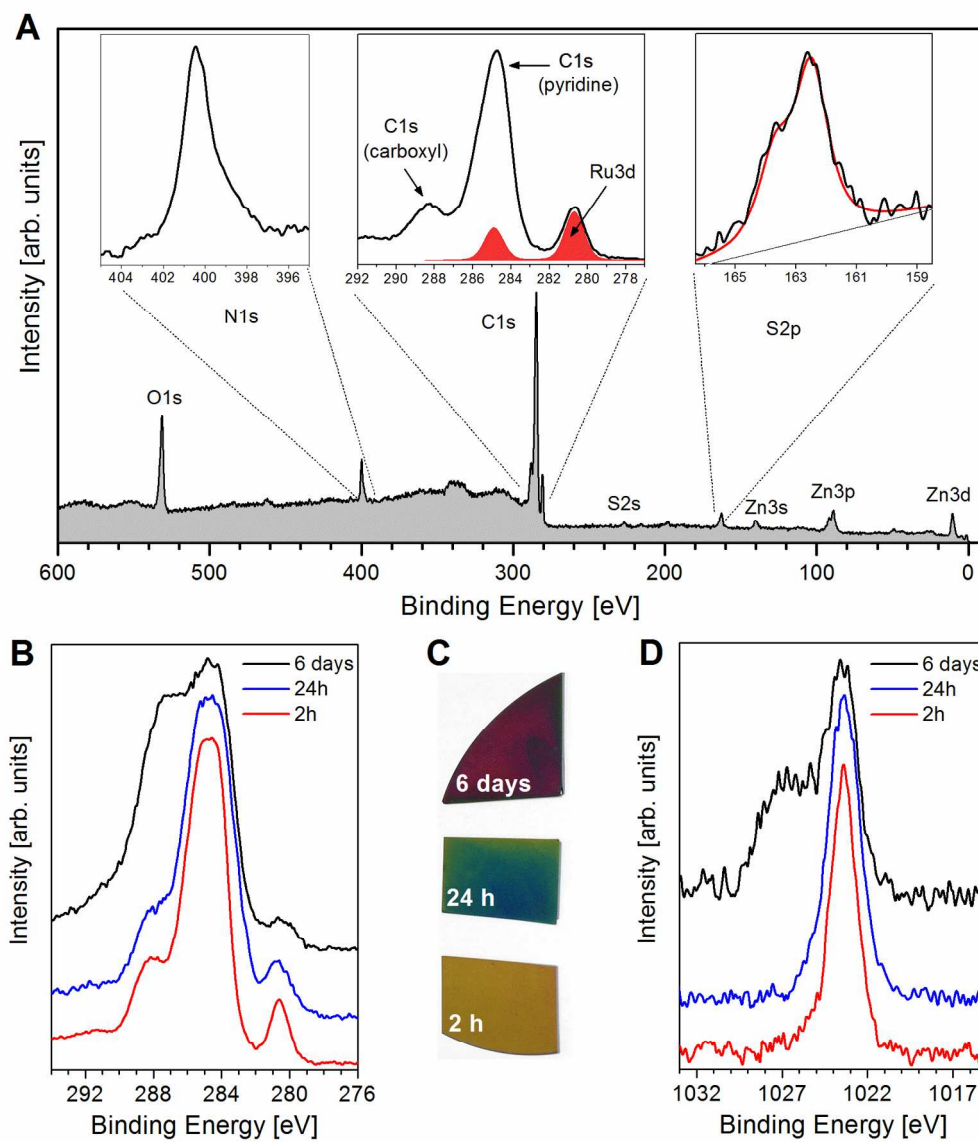
48. H. Horiuchi, R. Katoh, K. Hara, M. Yanagida, S. Murata, H. Arakawa and M. Tachiya, *The Journal of Physical Chemistry B*, 2003, 107, 2570-2574.
49. R. N. González-Moreno, P. L. Cook, I. Zegkinoglou, X. Liu, P. S. Johnson, W. Yang, R. E. Ruther, R. J. Hamers, R. n. Tena-Zaera, F. J. Himpsel, J. E. Ortega and C. Rogero, *The Journal of Physical Chemistry C*, 2011, 115, 18195-18201.
50. L. C. Mayor, J. Ben Taylor, G. Magnano, A. Rienzo, C. J. Satterley, J. N. O'Shea and J. Schnadt, *The Journal of Chemical Physics*, 2008, 129, 114701.
51. J. Chastain, J. F. Moulder and R. C. King, *Handbook of x-ray photoelectron spectroscopy: a reference book of standard spectra for identification and interpretation of XPS data*, Physical Electronics Division, Perkin-Elmer Corporation, 1995.
52. P. Persson and M. J. Lundqvist, *The Journal of Physical Chemistry B*, 2005, 109, 11918-11924.
53. M. Hahlin, E. M. J. Johansson, R. Schölin, H. Siegbahn and H. k. Rensmo, *The Journal of Physical Chemistry C*, 2011, 115, 11996-12004.
54. F. Yan, L. Huang, J. Zheng, J. Huang, Z. Lin, F. Huang and M. Wei, *Langmuir*, 2010, 26, 7153-7156.
55. M. Saes, F. van Mourik, W. Gawelda, M. Kaiser, M. Chergui, C. Bressler, D. Grolimund, R. Abela, T. E. Glover, P. A. Heimann, R. W. Schoenlein, S. L. Johnson, A. M. Lindenberg and R. W. Falcone, *Review of Scientific Instruments*, 2004, 75, 24-30.
56. F. A. Lima, C. J. Milne, D. C. V. Amarasinghe, M. H. Rittmann-Frank, R. M. van der Veen, M. Reinhard, V.-T. Pham, S. Karlsson, S. L. Johnson, D. Grolimund, C. Borca, T. Huthwelker, M. Janousch, F. van Mourik, R. Abela and M. Chergui, *The Review of Scientific Instruments*, 2011, 82, 063111.
57. A. M. March, A. Stickrath, G. Doumy, E. P. Kanter, B. Krässig, S. H. Southworth, K. Attenkofer, C. a. Kurtz, L. X. Chen and L. Young, *The Review of Scientific Instruments*, 2011, 82, 073110.
58. N. Bergeard, M. G. Silly, D. Krizmancic, C. Chauvet, M. Guzzo, J. P. Ricaud, M. Izquierdo, L. Stebel, P. Pittana, R. Sergo, G. Cautero, G. Dufour, F. Rochet and F. Sirotti, *Journal of Synchrotron Radiation*, 2011, 18, 245-250.
59. H. Bluhm, *Journal of Electron Spectroscopy and Related Phenomena*, 2010, 177, 71-84.
60. A. Oelsner, O. Schmidt, M. Schicketanz, M. Klais, G. Schönhense, V. Mergel, O. Jagutzki and H. Schmidt-Böcking, *Review of Scientific Instruments*, 2001, 72, 3968-3974.
61. A. Shavorskiy *et al.*, *Review of Scientific Instruments (to be submitted)*.
62. L. Kronik and Y. Shapira, *Surface Science Reports*, 1999, 37, 1-206.
63. A. Pietzsch, A. Föhlisch, F. Hennies, S. Vijayalakshmi and W. Wurth, *Appl. Phys. A*, 2007, 88, 587-592.
64. M. Kamada, J. Murakami, S. Tanaka, S. D. More, M. Itoh and Y. Fujii, *Surface Science*, 2000, 454-456, 525-528.
65. S. Tokudomi, J. Azuma, K. Takahashi and M. Kamada, *Journal of the Physical Society of Japan*, 2007, 76, 104710.
66. S. Tanaka, S. Dylan Moré, K. Takahashi and M. Kamada, *Journal of the Physical Society of Japan*, 2003, 72, 659-663.
67. A. Furube, R. Katoh, K. Hara, S. Murata, H. Arakawa and M. Tachiya, *The Journal of Physical Chemistry B*, 2003, 107, 4162-4166.
68. A. Furube, R. Katoh, T. Yoshihara, K. Hara, S. Murata, H. Arakawa and M. Tachiya, *The Journal of Physical Chemistry B*, 2004, 108, 12583-12592.
69. N. Anderson, J. Guo and T. Lian, *The journal of physical chemistry. B*, 2005, 109, 7088-7094.
70. G. Benkö, J. Kallioinen, P. Myllyperkiö, F. Trif, J. E. I. Korppi-Tommola, A. P. Yartsev and V. Sundström, *The Journal of Physical Chemistry B*, 2004, 108, 2862-2867.
71. J. Kallioinen, G. Benkö, V. Sundström, J. E. I. Korppi-Tommola and A. P. Yartsev, *The Journal of Physical Chemistry B*, 2002, 106, 4396-4404.
72. M. Pellnor, P. Myllyperkiö, J. Korppi-Tommola, A. Yartsev and V. Sundström, *Chemical Physics Letters*, 2008, 462, 205-208.
73. R. Katoh, A. Furube, T. Yoshihara, K. Hara, G. Fujihashi, S. Takano, S. Murata, H. Arakawa and M. Tachiya, *The Journal of Physical Chemistry B*, 2004, 108, 4818-4822.
74. C. Strothkämper, A. Bartelt, P. Sippel, T. Hannappel, R. Schütz and R. Eichberger, *The Journal of Physical Chemistry C*, 2013, 117, 17901-17908.
75. C. D. Pemmaraju and D. Pendergast, *private communication*.
76. S. B. Zhang, S. H. Wei and A. Zunger, *Physical Review B*, 2001, 63, 075205.



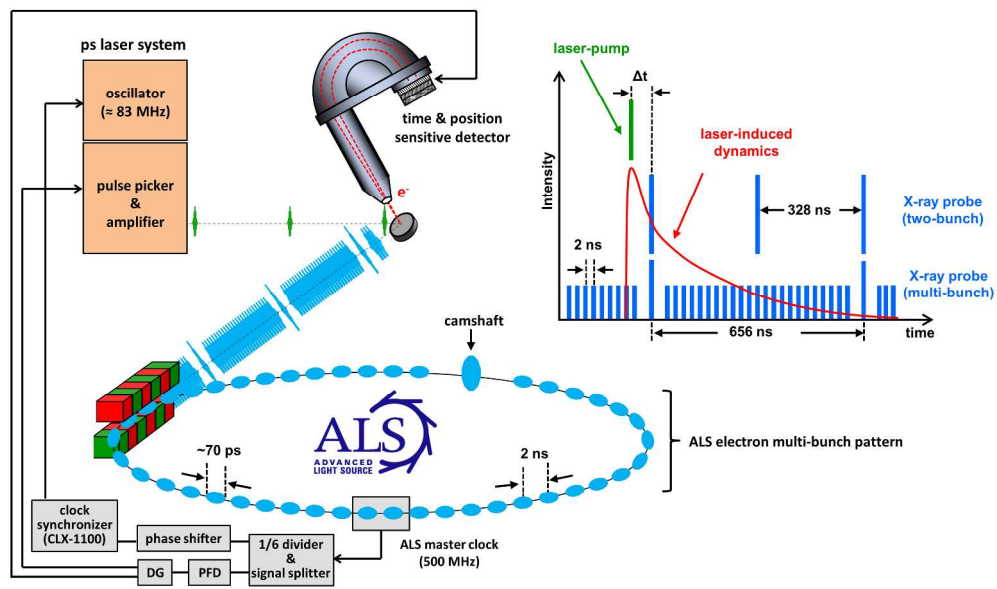
Electron dynamics at dye-semiconductor interfaces probed by picosecond time-resolved X-ray photoelectron spectroscopy
107x85mm (300 x 300 DPI)



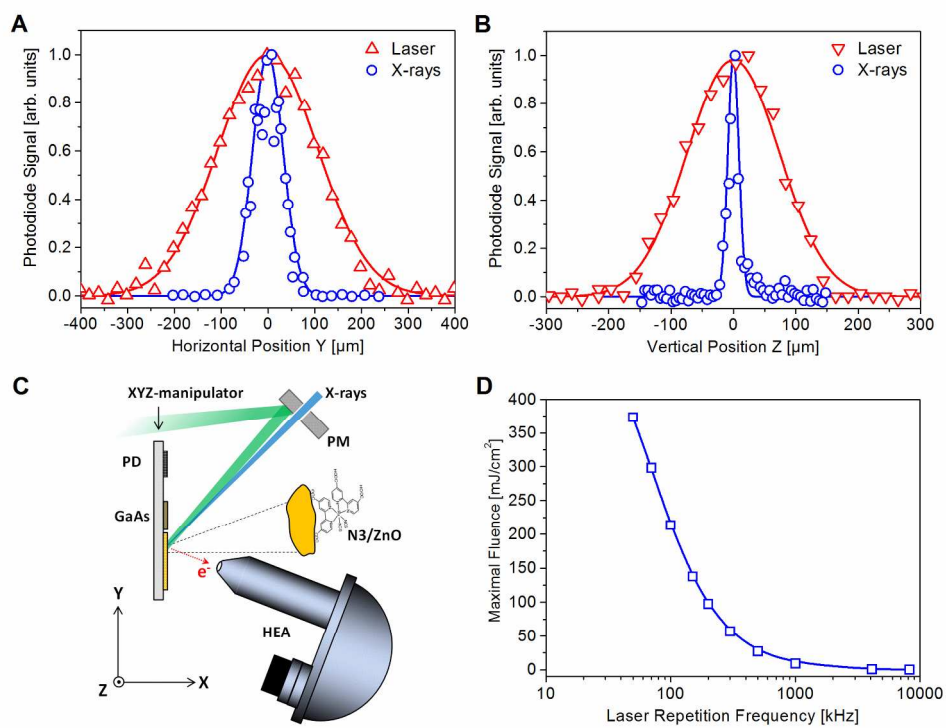
210x89mm (300 x 300 DPI)



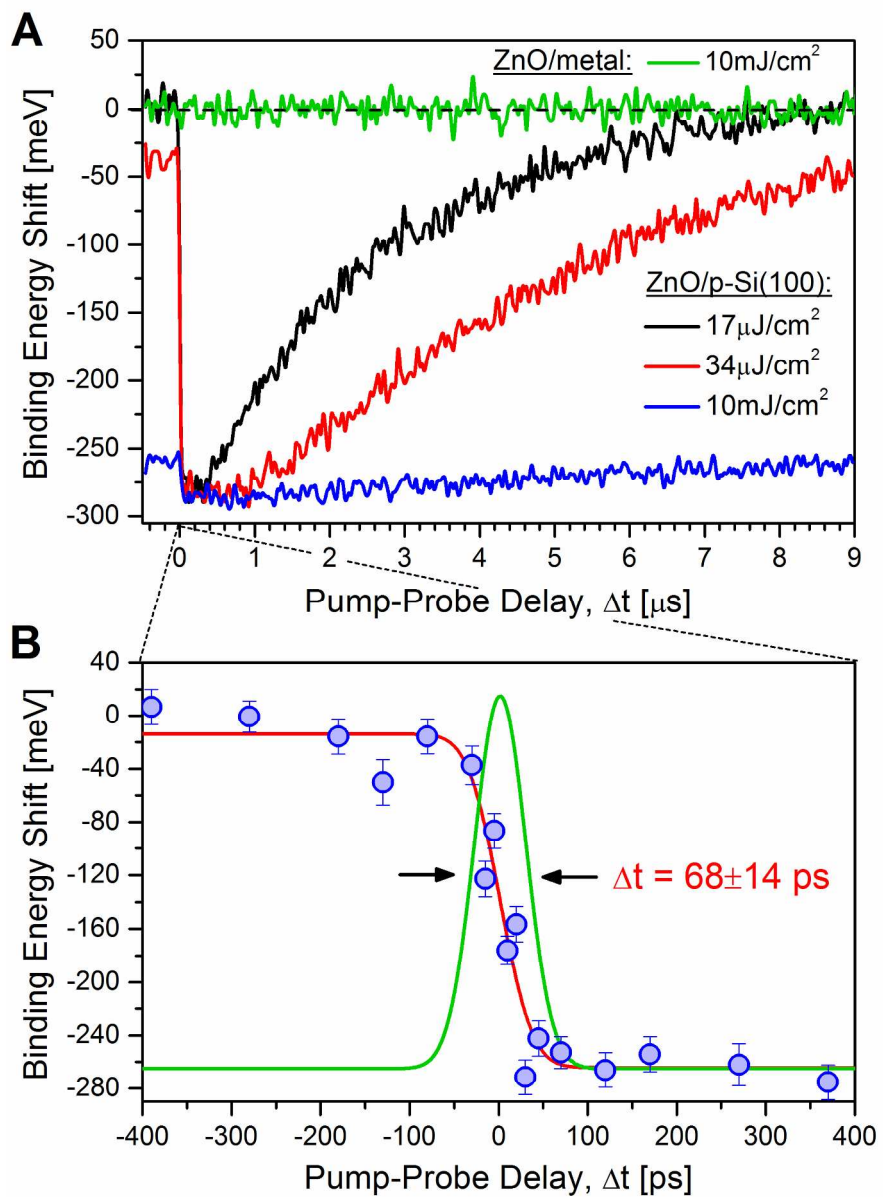
156x179mm (300 x 300 DPI)



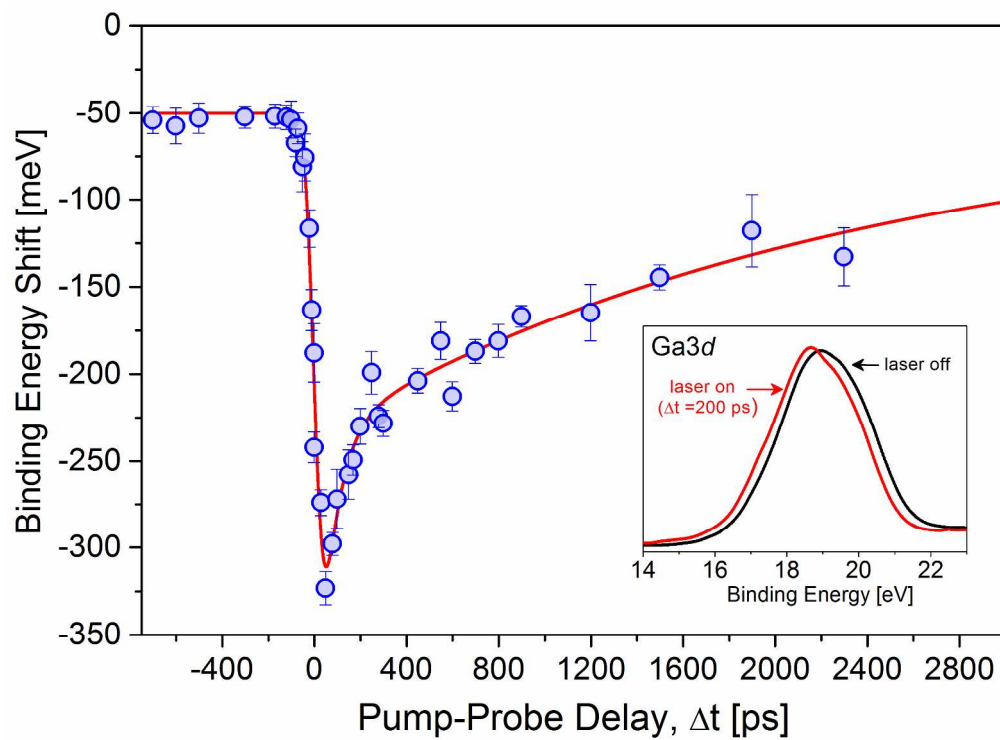
250x149mm (300 x 300 DPI)



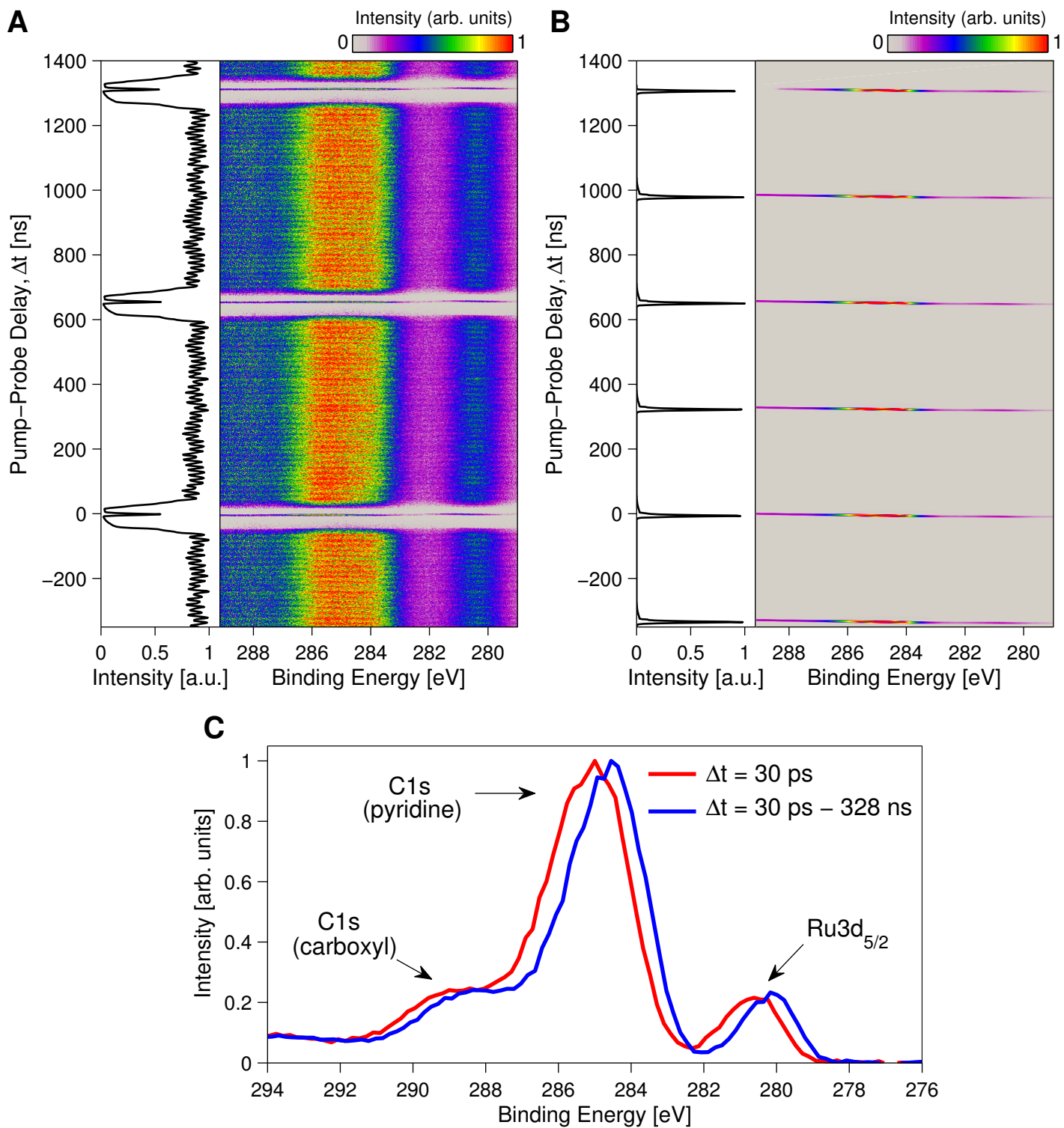
207x153mm (300 x 300 DPI)

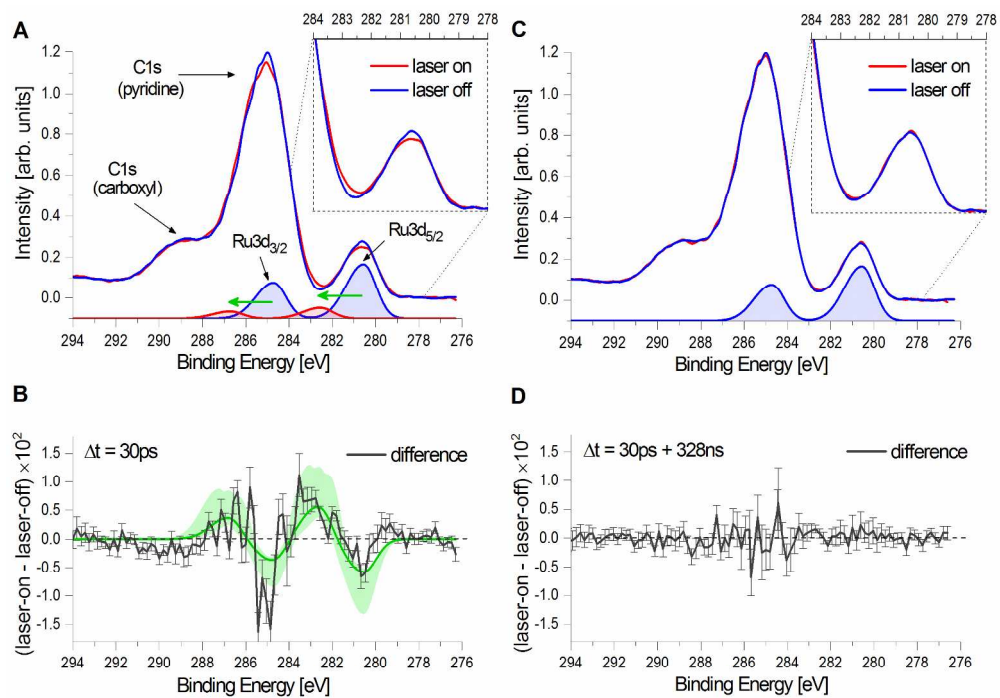


191x261mm (300 x 300 DPI)

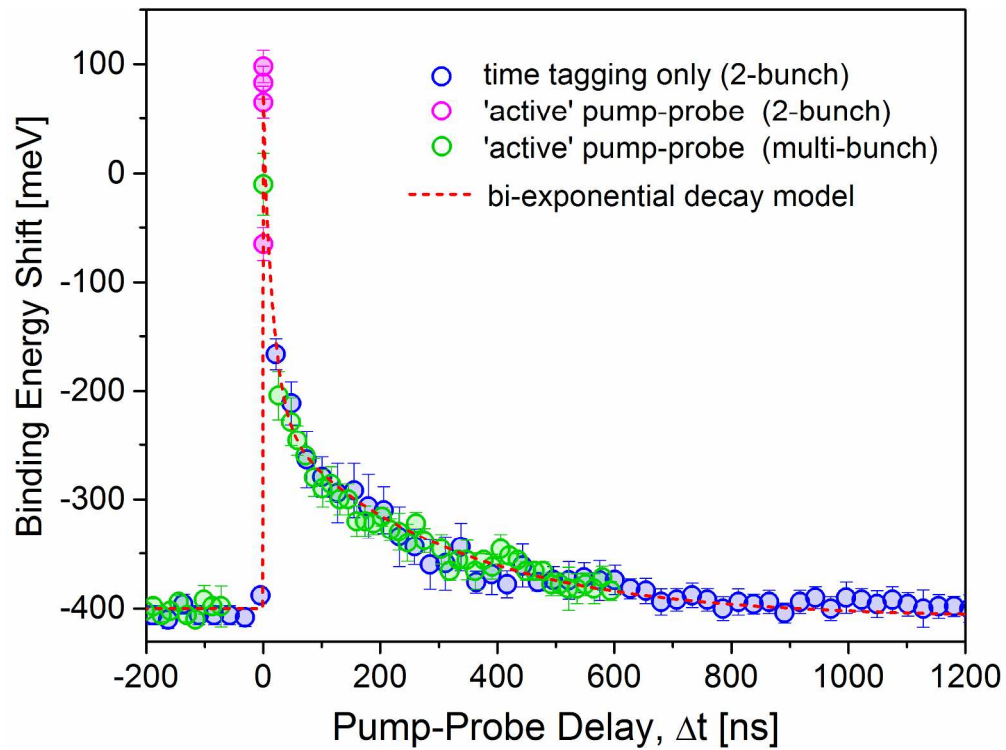


247x183mm (300 x 300 DPI)





255x193mm (300 x 300 DPI)



238x177mm (300 x 300 DPI)